

Cite this: *Chem. Sci.*, 2022, 13, 4010

All publication charges for this article have been paid for by the Royal Society of Chemistry

## Facile conversion of ammonia to a nitride in a rhenium system that cleaves dinitrogen†

Gannon P. Connor,<sup>a</sup> Daniel Delony,<sup>b</sup> Jeremy E. Weber,<sup>a</sup> Brandon Q. Mercado,<sup>a</sup> Julia B. Curley,<sup>a</sup> Sven Schneider,<sup>b</sup> James M. Mayer<sup>a</sup> and Patrick L. Holland<sup>a</sup>

Rhenium complexes with aliphatic PNP pincer ligands have been shown to be capable of reductive N<sub>2</sub> splitting to nitride complexes. However, the conversion of the resulting nitride to ammonia has not been observed. Here, the thermodynamics and mechanism of the hypothetical N–H bond forming steps are evaluated through the reverse reaction, conversion of ammonia to the nitride complex. Depending on the conditions, treatment of a rhenium(III) precursor with ammonia gives either a bis(amine) complex [(PNP)Re(NH<sub>2</sub>)<sub>2</sub>Cl]<sup>+</sup>, or results in dehydrohalogenation to the rhenium(III) amido complex, (PNP)Re(NH<sub>2</sub>)Cl. The N–H hydrogen atoms in this amido complex can be abstracted by PCET reagents which implies that they are quite weak. Calorimetric measurements show that the average bond dissociation enthalpy of the two amido N–H bonds is 57 kcal mol<sup>−1</sup>, while DFT computations indicate a substantially weaker N–H bond of the putative rhenium(IV)-imide intermediate (BDE = 38 kcal mol<sup>−1</sup>). Our analysis demonstrates that addition of the first H atom to the nitride complex is a thermochemical bottleneck for NH<sub>3</sub> generation.

Received 15th August 2021

Accepted 22nd February 2022

DOI: 10.1039/d1sc04503b

rsc.li/chemical-science

## Introduction

The interconversion of N<sub>2</sub> and NH<sub>3</sub> is important in fields that range from agriculture to sustainable energy.<sup>1,2</sup> The heavy use of NH<sub>3</sub> in fertilizer manufacturing has resulted in an extensive global infrastructure for its transportation and storage.<sup>3</sup> Coupled with its high energy density, this makes NH<sub>3</sub> an excellent candidate for a carbon-free chemical fuel, either through combustion or direct ammonia fuel cells (DAFCs).<sup>4–7</sup> In order to realize this potential, it is beneficial to understand the individual steps of N–N and N–H bond formation and cleavage. One promising route to form the N–H bonds in NH<sub>3</sub> from N<sub>2</sub> is proton-coupled electron transfer (PCET).<sup>8a,9</sup> Photo- or electrochemical energy may provide the necessary driving force for PCET-assisted N<sub>2</sub> reduction using water as a source of protons and electrons, thus providing a sustainable strategy for converting N<sub>2</sub> to NH<sub>3</sub>.<sup>10–16</sup> A growing number of homogeneous systems catalytically achieve this difficult transformation utilizing PCET.<sup>17–31</sup>

It is also important to understand the reverse reaction, NH<sub>3</sub> oxidation to form N<sub>2</sub>. One application of this reaction is for

releasing the chemical energy stored in N–H bonds for DAFC applications.<sup>6,7</sup> In addition, the individual steps in NH<sub>3</sub> oxidation to N<sub>2</sub> are often the microscopic reverse of those used for PCET reduction of N<sub>2</sub> and thus help to elucidate potential mechanisms for PCET-assisted reduction of N<sub>2</sub> to NH<sub>3</sub>.<sup>32</sup> In this context, it is relevant that many examples of chemical N–H bond oxidation from NH<sub>3</sub>-derived metal ammines yield metal nitride complexes.<sup>33–46</sup> These systems utilize either chemical oxidants under basic conditions or H-atom abstracting (HAA) reagents for the ammine-to-nitride transformations.<sup>8b</sup> In some systems, electrochemical oxidation of ammine complexes yields metal-nitride products.<sup>41,42,44</sup> Other systems can generate N<sub>2</sub> as a product from the oxidation of NH<sub>3</sub>-derived ammine complexes, either through chemical<sup>36,40,47–49</sup> or electrochemical<sup>49–52</sup> methods. These include recently reported homogeneous systems that catalytically form N<sub>2</sub> from NH<sub>3</sub> through both chemical<sup>43–45</sup> or electrochemical<sup>44,53–55</sup> N–H bond oxidation. N–N bond formation can occur *via* bimetallic N–N coupling (*e.g.*, between metal–NH<sub>x</sub> species or metal nitrides)<sup>40,44,45</sup> or nucleophilic attack on a metal–NH<sub>x</sub> intermediate by NH<sub>3</sub>.<sup>43,53,54,56</sup>

Here, we study NH<sub>3</sub> oxidation in a well-defined system that is also capable of reductive functionalization of N<sub>2</sub> *via* an N<sub>2</sub>-cleavage mechanism.<sup>57,58</sup> Electrochemical reduction of (PNP)ReCl<sub>2</sub> (**1**, PNP = N((CH<sub>2</sub>CH<sub>2</sub>)P<sup>t</sup>Bu<sub>2</sub>)<sub>2</sub>) cleaves N<sub>2</sub> to form the nitride complex (PNP)Re(N)Cl (**2**), which contains a nucleophilic nitride ligand (Scheme 1, black arrow).<sup>59–61</sup> This nitride can be alkylated and reduced to give N–C containing products,<sup>62,63</sup> but PCET reduction of the nitride in **2** to form NH<sub>3</sub>

<sup>a</sup>Department of Chemistry, Yale University, New Haven, Connecticut, USA. E-mail: patrick.holland@yale.edu

<sup>b</sup>Institute of Inorganic Chemistry, Georg-August-Universität Göttingen, Göttingen, Germany

† Electronic supplementary information (ESI) available: Details of synthesis, electrochemistry, calorimetry, computations, and crystallography; spectra. CCDC 2100974 and 2100975. For ESI and crystallographic data in CIF or other electronic format see DOI: 10.1039/d1sc04503b



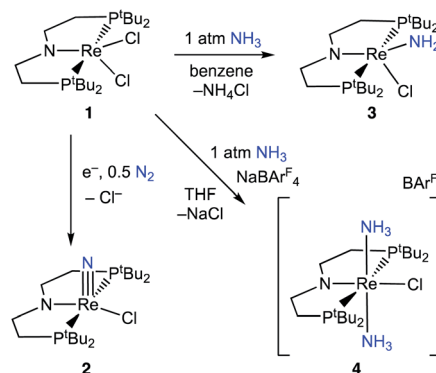
**Scheme 1** Cycles that represent reductive  $N_2$  splitting by (PNP)Re and PCET nitride reduction (gray cycle, not observed) or  $NH_3$  oxidation (blue cycle, studied here).

(Scheme 1, grey arrows) was not observed because pincer protonation occurs rather than nitride protonation. Additional challenges are that the high energy of the lowest unoccupied molecular orbital (LUMO) of **2** prevents a reduction-first pathway, and that **2** is unreactive towards organic hydrogen-atom transfer (HAT) reagents or  $H_2$ .<sup>59</sup> In this manuscript, we evaluate the reverse reactions (Scheme 1, blue arrows) to elucidate the factors that prevent PCET nitride reduction in this system. This fundamental information may help to improve  $NH_3$  oxidation catalysis and to avoid bottlenecks in  $NH_3$  generation by future  $N_2$ -cleaving systems, and importantly provides a thermochemical framework for nitrogen fixation products beyond ammonia.

## Results

### Binding and deprotonation of $NH_3$

Introduction of 1 atm of  $NH_3$  gas to a solution of the dichloride complex **1** in benzene- $d_6$  or tetrahydrofuran- $d_8$  (THF- $d_8$ ) results in an immediate color change from purple to brown.  $^1H$  NMR spectroscopy reveals the formation of a new  $C_s$ -symmetric product **3** in >95% yield (Scheme 2, top). The chemical shifts of **3** (Fig. S1†) are characteristic of a non-magnetic ground state non-, and the lack of noticeable temperature-independent paramagnetism, which is often observed in  $Re^{III}$  complexes,<sup>64,65</sup> suggests that the two strongly  $\pi$ -donating amide ligands sufficiently destabilize the spin triplet state to give a well-isolated singlet ground state. A notable  $^1H$  resonance integrating to 2H is found at  $\delta$  12.7 ppm. A  $^1H$ - $^{15}N$  HSQC spectrum of a natural-abundance sample shows a  $^{15}N$  cross-peak from this resonance at  $\delta$  -260 ppm (Fig. S2†), confirming that it corresponds to protons bound to N. This  $^{15}N$  chemical



**Scheme 2** Reactivity of **1** with  $N_2$  and  $NH_3$ .

shift is significantly upfield from related nitride complexes (371–393 ppm) and closer to that for the protonated PNP backbone of  $[(^1H)PNP]Re(N)Cl]^+$  (**5**) (–336 ppm).<sup>66</sup> All spectroscopic signatures are consistent with the formulation of **3** as the amido complex  $(PNP)Re(NH_2)Cl$ .

On a preparative scale, addition of 1 atm  $NH_3$  to a solution of **1** gives **3** as the major product, which is isolated from the reaction in 61% yield. The solid-state structure of **3** was elucidated *via* single crystal X-ray diffraction (XRD) and the N-bound hydrogen atoms were located in the Fourier map (Fig. 1). The Re– $NH_2$  bond in **3** is 0.3 Å longer than the  $Re\equiv N$  bond in the nitride complex **2** (Table 1).<sup>66</sup> In the supporting ligand, the (PNP)–Re bond is 0.1 Å shorter in **3** than in the Re–nitride complex **2**, indicating increased  $\pi$ -bonding from the nitrogen of the pincer ligand in **3** (Table 1). The (PNP)–Re and Re– $NH_2$  amide bond lengths in **3** are within 0.02 Å of each other with

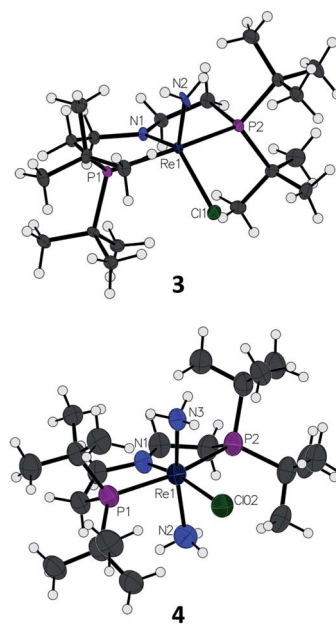


**Fig. 1** Solid-state structures of Re–amide complex **3** and  $Re(NH_3)_2$  complex **4** ( $BARF_4$  ion omitted) with thermal ellipsoids at 50% probability.

**Table 1** Selected bond lengths (Å) and bond angles (°) of complexes 2–4

Bond/angle	2	3	4
Re1–N1	2.033(6)	1.936(3)	1.894(5)
Re1–N2	1.643(6)	1.959(3)	2.150(5)
Re1–N3	—	—	2.193(6)
Re1–Cl1	2.441(2)	2.384(1)	2.495(2)
Re1–P1	2.443(2)	2.397(1)	2.424(2)
Re1–P2	2.435(2)	2.382(1)	2.425(2)
N1–Re1–N2	105.8(3)	115.5(1)	84.8(2)
N1–Re1–N3	—	—	165.6(2)
N2–Re1–N3	—	—	109.6(2)
N1–Re1–Cl1	106.5(2)	108.8(1)	83.4(1)
N2–Re1–Cl1	147.7(2)	135.6(1)	167.0(2)
N1–Re1–P1	100.4(2)	95.1(1)	91.0(1)
N1–Re1–P2	99.9(2)	95.5(1)	90.5(1)

planar coordination of the nitrogen atoms in both cases ( $\Sigma_{\text{PNP}} = 360^\circ$ ,  $\Sigma_{\text{NH}_2} = 357^\circ$ ). The PNP and  $\text{NH}_2$  amides are oriented to  $\pi$ -donate into the same Re d orbital, which gives modest lengthening (0.04 Å) of the (PNP)–Re bond in **3** compared to the Re-dichloride complex **1**.<sup>59</sup> This also likely contributes to increased pyramidalization of the dialkylamide group ( $\Sigma_{\text{PNP}} = 348^\circ$ ) in **2**. These structural differences are accompanied by a change of the rhenium coordination geometry from square pyramidal ( $\tau_5 = 0.14$ ) in complex **2**, in which the coordination site *trans* to the nitride is open, toward trigonal bipyramidal ( $\tau_5 = 0.48$ ) in complex **3**.

When 1 equiv. of  $\text{NH}_3$  gas was added to a solution of **1** in THF- $d_8$  at  $-80^\circ\text{C}$ ,  $^1\text{H}$  and  $^{31}\text{P}\{^1\text{H}\}$  NMR spectra of the reaction showed a mixture of diamagnetic products (Fig. 2, middle). Addition of another 4 equiv. of  $\text{NH}_3$  gas (for a total of 5 equiv.  $\text{NH}_3$  per Re) resulted in full consumption of **1** and observation of **3** in 71% yield (Fig. 2, top). It is likely that dehydrohalogenation of the putative intermediate (PNP)Re( $\text{NH}_3$ )Cl<sub>2</sub> by  $\text{NH}_3$  to form  $\text{NH}_4\text{Cl}$  is required to drive the formation of **3**. This implies that coordination to  $\text{Re}^{\text{III}}$  significantly increases the acidity of the N-bound protons.<sup>67</sup>

Addition of 1 atm  $\text{NH}_3$  to a solution of **1** containing an equivalent of  $\text{NaBar}^{\text{F}}_4$  ( $\text{Ar}^{\text{F}} = 3,5\text{-bis(trifluoromethyl)phenyl}$ ) in

THF- $d_8$  at  $-80^\circ\text{C}$  resulted in a color change from purple to light green and formation of the new diamagnetic complex **4** by  $^1\text{H}$  and  $^{31}\text{P}\{^1\text{H}\}$  NMR spectroscopy (see Scheme 2). In contrast to **3**, complex **4** exhibits  $C_{2v}$  symmetry, broadened resonances, and a new peak at  $\delta = 5.47$  ppm that integrates to 6H (Fig. S3†). Despite no identifiable cross-peaks in the  $^1\text{H}$ – $^{15}\text{N}$  HSQC spectrum of **4**, N–H stretching bands were observed in the infrared (IR) spectrum at 3392, 3353, 3245, and 3174  $\text{cm}^{-1}$ . The molecular structure of **4** in the solid state shows the six-coordinate, cationic bis-ammine adduct [(PNP)Re( $\text{NH}_3$ )<sub>2</sub>Cl][ $\text{Bar}^{\text{F}}_4$ ] with a distorted octahedral geometry (Fig. 1). In comparison to **3**, complex **4** shows lengthened Re–N bonds (2.172(5) Å vs. 1.959(3) Å) due to the lack of  $\pi$ -donation. With no strong  $\pi$ -donor ligands to compete with  $\pi$ -donation from the PNP amide, **4** contains a Re–PNP bond distance that is shorter than in **3** and **2** (Table 1). The flexibility of the PNP–Re interaction to accommodate the changes in ligand donor characteristics from ammine to nitride is also evident from the change in the PNP–Re bond lengths and PNP pyramidalization from **2**–**4**.

### Reactivity of [(PNP)Re( $\text{NH}_3$ )<sub>2</sub>Cl]<sup>+</sup>

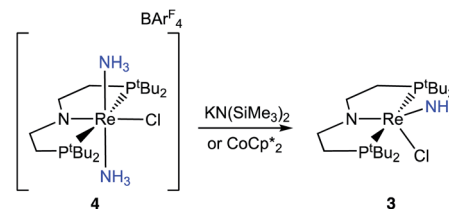
To assess the plausibility of an ammine complex as an intermediate during formation of **3**, a solution of **4** in THF- $d_8$  was treated with 1 atm of  $\text{NH}_3$ , which gave no reaction. However, addition of a slight excess of potassium hexamethyldisilazide (KHMDs) (Scheme 3) caused an immediate color change and formation of **3** as the major product in 61% yield, as judged by  $^1\text{H}$  and  $^{31}\text{P}\{^1\text{H}\}$  spectroscopy (Fig. S4†).

Cyclic voltammetry (CV) of **4** in THF under Ar shows irreversible redox processes, a reduction at  $E_{\text{pc}} = -1.95$  V vs.  $\text{Cp}_2\text{Fe}^{+/0}$  and an oxidation at  $E_{\text{pa}} = -0.58$  V vs.  $\text{Cp}_2\text{Fe}^{+/0}$  (Fig. S16†). The position of the reduction peak is similar to the reversible reduction of **1** under Ar at  $-2.00$  V vs.  $\text{Cp}_2\text{Fe}^{+/0}$ .<sup>68</sup> The first reduction of **1** under Ar was previously attributed to the formation of [(PNP)Re<sup>II</sup>Cl<sub>2</sub>]<sup>–</sup>, which is followed by chloride dissociation to form (PNP)Re<sup>II</sup>Cl which is subsequently reduced again.<sup>60</sup> The difficulty of reducing **4** suggests that it is quite electron-rich despite its positive charge, but the lack of reversibility prevents further interpretation.

In an attempt to assess the species formed upon reduction, **4** was treated with a chemical reductant. Addition of 1.2 equiv.  $\text{CoCp}^*_2$  to a solution of **4** in THF- $d_8$  under  $\text{N}_2$  gave complete consumption of **4** but the Re amide **3** was formed (Fig. S5†). The spectroscopic yield of **3** was only 60%. The fate of the lost proton and electron in the formation of **3** remain unknown. Analysis of



**Fig. 2**  $^1\text{H}$  and  $^{31}\text{P}\{^1\text{H}\}$  NMR spectra of **1** in THF- $d_8$  without  $\text{NH}_3$  (bottom, maroon), with 1 equiv.  $\text{NH}_3$  added (middle, green), and with 5 equiv.  $\text{NH}_3$  added (top, blue). Spectroscopic yields reported vs.  $\text{PMe}_3$  in a capillary.



**Scheme 3** Reactivity of **4** with stoichiometric base or reductant.

the headspace following the reaction showed no detectable amount of  $H_2$  (<1% yield).

### N–H abstraction from Re–amide complex (PNP)Re(NH<sub>2</sub>)Cl

We hypothesized that abstraction of H atoms from **3** would lead to the nitride (Scheme 1, blue), by analogy with other reported systems.<sup>37–40,43,45,46</sup> In the following, we assume that formal H<sup>•</sup> abstraction by the hydrogen atom abstraction (HAA) reagents is most likely concerted, based on the known difficulty of stepwise PCET pathways.<sup>8</sup> Addition of 2 equiv. of either 2,4,6-*tert*-butylphenoxyl radical (<sup>t</sup>Bu<sub>3</sub>PhO<sup>•</sup>) or 2,2,6,6-tetramethylpiperidine 1-oxyl (TEMPO<sup>•</sup>) as HAA reagents to a solution of **3** in THF-*d*<sub>8</sub> or benzene-*d*<sub>6</sub> at ambient temperature gives rapid and quantitative (>99%) formation of **2** (Scheme 4), as judged by <sup>1</sup>H and <sup>31</sup>P{<sup>1</sup>H} NMR spectroscopy (Fig. S6†). This is accompanied by the formation of 2 equiv. of <sup>t</sup>Bu<sub>3</sub>PhOH or TEMPOH. These reagents have O–H bond dissociation free energies (BDFE<sub>O–H</sub>) of 74.4 and 65.5 kcal mol<sup>–1</sup> in THF, respectively.<sup>8b,69</sup> When **3** is mixed with only 1 equiv. of TEMPO<sup>•</sup>, only half of **3** is consumed, showing that the second H-atom abstraction is more favorable than the first (Fig. S7†). The absence of reactivity of **2** with excess <sup>t</sup>Bu<sub>3</sub>PhOH or TEMPOH supports this notion.

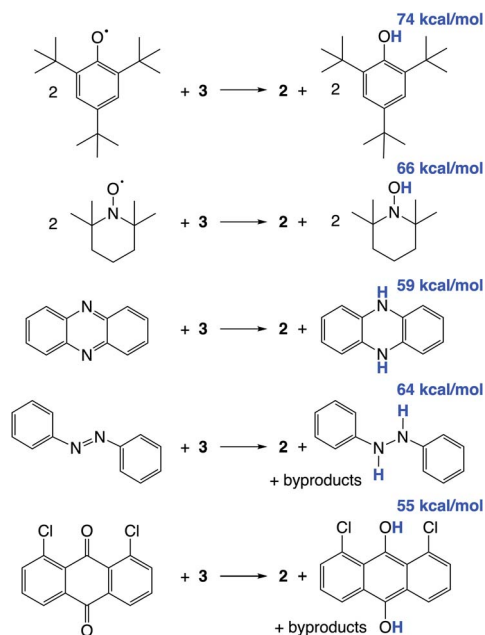
Additional HAA reagents were used to further bracket the N–H bond strengths (Scheme 4). While **3** did not react with 5,10-phenazine (5 equiv) in THF-*d*<sub>8</sub> at ambient temperature, heating to 80 °C gave quantitative (>98%) conversion to **2** and 5,10-dihydrophenazine (average BDFE<sub>N–H</sub> = 58.7 kcal mol<sup>–1</sup> in MeCN<sup>69</sup>) after 21 h (Fig. S8†). Accordingly, no reaction was observed between **2** and 10 equiv. of 5,10-dihydrophenazine even after prolonged heating at 80 °C. Oxidation of **3** to form **2** was also observed when using 1.5 equiv. of azobenzene (54% yield of **2** after 72 h at 60 °C) and 1,8-dichloro-9,10-

anthraquinone (67% yield of **2** after 4 d at ambient temperature). <sup>1</sup>H NMR spectra of reaction mixtures showed the formation of 1,2-diphenylhydrazine and 1,8-dichloro-9,10-anthracenediol (average BDFE<sub>X–H</sub> = 60.9 [in MeCN] and 55.4 kcal mol<sup>–1</sup> [THF]), respectively.<sup>69</sup> However, these reactions form multiple products, so quantitative thermochemical information cannot be derived from the product formation in these cases. Quantification of the PCET thermochemistry was therefore carried out by titration calorimetry as detailed below.

### Stepwise ET–PT from (PNP)Re(NH<sub>2</sub>)Cl

The reactivity of **3** with HAA reagents suggests that the N–H bonds in the amide ligand can be easily oxidized *via* concerted removal of an H-atom.<sup>8</sup> We were also interested to determine whether the conversion to **2** is possible through stepwise PCET, with deprotonation and 1e<sup>–</sup> oxidation of **3**.<sup>41,42,44</sup> In order to test a PT–ET (proton transfer followed by electron transfer) pathway, a solution of **3** was mixed with up to 12 equiv. of 1,8-diazabicyclo[5.4.0]undec-7-ene (DBU, pK<sub>a</sub> of conjugate acid = 16.9), phosphazene base P<sub>1</sub>-tBu-tris(tetramethylene) (pK<sub>a</sub> of conjugate acid = 20.2), or phosphazene base P<sub>4</sub>-tBu (pK<sub>a</sub> of conjugate acid = 33.9) in THF-*d*<sub>8</sub> at ambient temperature.<sup>70</sup> No reaction of **3** with any of these strong bases was observed by <sup>1</sup>H and <sup>31</sup>P{<sup>1</sup>H} NMR spectroscopy, indicating that the amide ligand in **3** is a poor Brønsted acid.

In other tests, we explored whether a stepwise ET–PT pathway (electron transfer followed by proton transfer) is feasible. CV of **3** in THF shows an irreversible oxidation wave (*E*<sub>pa</sub> = –0.61 V vs. Cp<sub>2</sub>Fe<sup>+/0</sup>) at a scan rate of 100 mV s<sup>–1</sup> (Fig. 3). However, increasing the scan rate to 1 V s<sup>–1</sup> results in a distinct anodic shift of the oxidation event and increased reversibility, indicating chemical follow-up steps at a time-scale of the CV experiment. This potential is similar to those for the oxidation of both the dichloride complex **1** and the Re(NH<sub>3</sub>)<sub>2</sub> complex **4**.<sup>60</sup> Further analysis of the CV has not been fruitful because of the lack of reversibility and formation of unknown byproducts (see below). However, electrolysis of a solution of **3** in the presence of 2,6-lutidine (pK<sub>a</sub> = 7.2 in THF<sup>70</sup>) at a potential of +0.6 V relative to the open circuit potential (OCP) resulted in steady passing of charge up to 2.2 equiv. e<sup>–</sup> (Fig. S15†) and a change in color from



**Scheme 4** Reactivity of **3** with organic HAA reagents, with BDFE<sub>O–H</sub> or average BDFE<sub>X–H</sub> of the organic products in THF given in blue.



**Fig. 3** Cyclic voltammogram of the first oxidation of **3** (0.2 mM) in 0.2 M NBu<sub>4</sub>PF<sub>6</sub> solution in THF under N<sub>2</sub> using a glassy carbon working electrode, Pt wire auxiliary electrode, and Ag wire pseudoreference. Potentials referenced to Cp<sub>2</sub>Fe<sup>+/0</sup> after the experiments.



brown to orange. Rhenium(v) nitride complex **5**, in which the backbone is protonated,<sup>66</sup> was isolated from the post-electrolysis mixture in 69% isolated yield (Fig. S17†). The combination of removing an electron at  $-0.61$  V and a proton with lutidine is thermodynamically equivalent to an “effective BDFE” of  $56 \text{ kcal mol}^{-1}$ ,<sup>69,71</sup> so this  $e^-/H^+$  removal is thermodynamically similar to the HAA reactions above.

In an effort to identify oxidation products of **3**, chemical oxidation was carried out with 1.1 equiv. of  $[\text{Cp}_2\text{Fe}][\text{PF}_6]$  in  $\text{THF}-d_8$  (Scheme 5). The major product identified from the resulting  $^1\text{H}$  and  $^{31}\text{P}\{^1\text{H}\}$  NMR spectra was **5** in 50% yield (Fig. S9†).<sup>66</sup> Furthermore, the  $\text{Re}^{\text{III}}$ -dichloride complex **1** was obtained in 25% yield, as well as a brown precipitate that could not be identified. The formation of both  $\text{Re}^{\text{III}}$  and  $\text{Re}^{\text{V}}$  complexes from the  $1e^-$  oxidation of **3** implies disproportionation; however, these products are not formed in a 1 : 1 ratio, implicating additional decomposition pathways. The product mixture that can be identified spectroscopically does not account for all of the Re, N, or H atoms present in the starting material. To test whether the missing H atoms could be released as  $\text{H}_2$  from weakened N–H bonds during the reaction, the reaction was repeated on a larger scale. Analysis of the  $\text{THF}$ -soluble products from the reaction showed formation of **1** and **5** in 17% and 52% yield, respectively, and no  $\text{H}_2$  was detected from analysis of the headspace (<1% yield).

We also tested whether oxidation of **3** to a nitride could be facilitated by providing an exogenous base for the deprotonation steps and by using 2 equiv. of oxidant (Scheme 5). Accordingly, 20 equiv. 2,6-lutidine and 2.2 equiv.  $[\text{Cp}_2\text{Fe}][\text{PF}_6]$  were added to a solution of **3** in  $\text{THF}-d_8$ , forming **5** in 82% spectroscopic yield, and no observable **1** (Fig. S10†). An unidentified brown solid was formed as a byproduct in both reactions, suggesting decomposition. The formation of unknown byproducts deterred us from further mechanistic analysis.

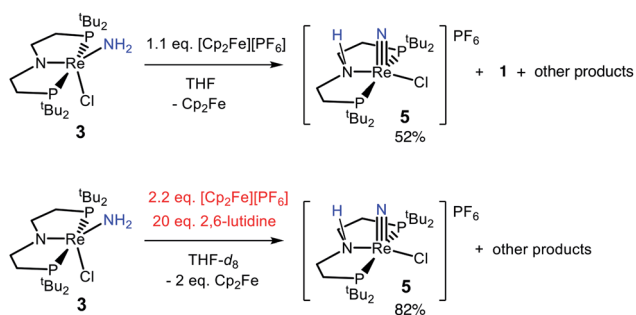
### Calorimetric measurement and DFT calculations of N–H bond oxidation from $(\text{PNP})\text{Re}(\text{NH}_2)\text{Cl}$

Since the reaction of **3** with 2 equiv.  ${}^t\text{Bu}_3\text{PhO}^\bullet$  to form **2** and 2 equiv.  ${}^t\text{Bu}_3\text{PhOH}$  proceeds quantitatively, we chose this reaction for calorimetric determination of the reaction enthalpy.<sup>72,73</sup> The

titration of **3** with  ${}^t\text{Bu}_3\text{PhO}^\bullet$  in  $\text{THF}$  using isothermal titration calorimetry (ITC) results in an exotherm of  $-50.9 \text{ kcal mol}^{-1}$  until 2.0 equiv. of  ${}^t\text{Bu}_3\text{PhO}^\bullet$  are added (Fig. S18†).<sup>33,73</sup> Thus, on average, each abstraction of an H atom from **3** gives an enthalpy change of  $-25.4 \text{ kcal mol}^{-1}$ . Since the bond dissociation enthalpy of  ${}^t\text{Bu}_3\text{PhO}-\text{H}$  in  $\text{THF}$  is  $80.8 \pm 1 \text{ kcal mol}^{-1}$ ,<sup>‡</sup> the average of the two  $\text{BDE}_{\text{N}-\text{H}}$  values of **3** in  $\text{THF}$  is  $55.4 \pm 1 \text{ kcal mol}^{-1}$ .

DFT calculations were used to obtain more insight into the thermodynamics of each PCET step from amide complex **3** to nitride complex **2**. The B3LYP functional and def2-TZVP basis, together with standard solvent and dispersion corrections gave excellent agreement with the metrical parameters of the crystal structure of **3**, and predicted the redox potential for  $3^{+/0}$  ( $E = -0.65 \text{ V}$ ) close to the observed wave at  $-0.61 \text{ V}$  in the experimental CV (see ESI†). Computation of the putative PCET intermediate confirmed that the  $S = 1/2$   $\text{Re}^{\text{IV}}$ -imide  $(\text{PNP})\text{Re}(\text{NH})\text{Cl}$  (**LRe=NH**) is the most stable tautomer; an isomeric amido-rhenium(IV) complex,  $(\text{PNP}^*)\text{Re}(\text{NH}_2)\text{Cl}$  ( $\text{PNP}^* = \text{N}(\text{CHCH}_2\text{-P}^t\text{Bu}_2)(\text{CH}_2\text{CH}_2\text{P}^t\text{Bu}_2)$ ), with an unsaturated PNP backbone proved higher in free energy by  $12 \text{ kcal mol}^{-1}$ . The optimized structure of **LRe=NH** shows a strongly bent parent imido ligand with a computed  $\text{Re}-\text{N}-\text{H}$  angle of  $133^\circ$ . Bending reduces the antibonding  $\pi$ -interaction of the multiply bonding imido ligand with the metal centred SOMO after reduction. In consequence, the Re–imide bond is considerably elongated ( $1.80 \text{ \AA}$ ) with respect to the parent nitride (DFT:  $1.66 \text{ \AA}$ ).

Computations of the *enthalpies* associated with each sequential H-atom transfer from **3** to  ${}^t\text{Bu}_3\text{PhO}^\bullet$  to give  ${}^t\text{Bu}_3\text{PhOH}$  in  $\text{THF}$  gave an average calculated  $\text{BDE}_{\text{N}-\text{H}}$  of  $57 \text{ kcal mol}^{-1}$  (Scheme 6).<sup>38,40,58</sup> This is close to the calorimetrically determined average BDE of  $55.4 \pm 1 \text{ kcal mol}^{-1}$ . The *free energy* of conversion of **3** to **2** via H-atom transfer to  ${}^t\text{Bu}_3\text{PhO}^\bullet$  gave an average calculated  $\text{BDFE}_{\text{N}-\text{H}}$  in **3** of  $51 \text{ kcal mol}^{-1}$ . Further insight comes from the hypothetical  $1e^-/1H^+$  steps. The  $\text{BDFE}_{\text{N}-\text{H}}$  for removing the first H from the amide ligand in **3** was calculated to be  $69 \text{ kcal mol}^{-1}$ , which is substantially higher than the computed  $\text{BDFE}_{\text{N}-\text{H}}$  of the second N–H bond (in **LRe=NH**),  $33 \text{ kcal mol}^{-1}$ . These computations show that the N–H bond in **LRe=NH** is particularly weak, which is consistent with both the facile, irreversible oxidation of **3** with HAA reagents and the inability to observe this putative parent imido complex (see ESI†).



Scheme 5 Reactions of **3** with chemical oxidants.



Scheme 6 DFT (B3LYP/def2-TZVP) computed thermochemistry for the oxidation of **3** to **2** via stepwise H-atom removal.



**Table 2** Comparison of the measured average N–H bond dissociation enthalpy in **3** to computed N–H bond dissociation free energies (BDFE) of NH<sub>x</sub> ligands in other relevant systems

Complex	Solvent	BDFE <sub>N–H</sub> (kcal mol <sup>−1</sup> )			Reference
		NH <sub>3</sub>	NH <sub>2</sub>	NH	
(PNP)Re(NH <sub>x</sub> )Cl ( <b>3</b> , computed)	THF	—	69	33	This work
(PNP)Re(NH <sub>x</sub> )Cl ( <b>3</b> , experimental)	THF	—	57(ave) <sup>a</sup>	—	This work
<i>cis</i> -(PONOP)Re(NH <sub>x</sub> )Cl <sub>2</sub>	THF	—	78	43	58
(PNP)Ir(NH <sub>x</sub> )	Gas phase	—	95 <sup>a</sup>	71 <sup>a</sup>	46
<i>trans</i> -[(Ph-tpy)(PPh <sub>2</sub> Me) <sub>2</sub> Mo(NH <sub>x</sub> )] <sup>+</sup>	THF	46	64	—	74 and 75
<i>cis</i> -[(Cp)(P <sup>Ph</sup> <sub>2</sub> N <sup>tBu</sup> <sub>2</sub> )Mo(NH <sub>x</sub> )(CO)] <sup>+</sup>	Et <sub>2</sub> O	84	61	—	38
[(PY5)Mo(NH <sub>x</sub> )] <sup>2+</sup>	MeCN	68	65	64	40
[(Cp*)(P <sup>tBu</sup> <sub>2</sub> N <sup>Ph</sup> <sub>2</sub> )Ru(NH <sub>x</sub> )] <sup>+</sup>	THF	83	89	72	43
[(tpy)( <sup>NMe2</sup> bpy)Ru(NH <sub>x</sub> )] <sup>2+</sup>	THF	79	86	—	56
(TMP)Ru(NH <sub>x</sub> ) <sub>2</sub>	C <sub>6</sub> H <sub>6</sub>	82	93	75	45
[(tpy)( <sup>NMe2</sup> bpy)Fe(NH <sub>x</sub> )] <sup>2+</sup>	THF	82	90	—	56
[( <sup>Ph</sup> NCH <sub>2</sub> CH <sub>2</sub> ) <sub>3</sub> N]Mo(NH <sub>x</sub> )	—	52	64	42	76
[(BP <sub>3</sub> )Fe(NH <sub>x</sub> )] <sup>+</sup>	Et <sub>2</sub> O	—	80	65	77
(F)(H <sub>2</sub> PCH <sub>2</sub> CH <sub>2</sub> PH <sub>2</sub> ) <sub>2</sub> Mo(NH <sub>x</sub> )	Benzene	41	92	37	78
(salen)Mn(NH <sub>x</sub> )	Gas phase	85	84	60	79
(η <sup>5</sup> -C <sub>5</sub> Me <sub>4</sub> SiMe <sub>3</sub> ) <sub>2</sub> Ti(NH <sub>x</sub> )	Gas phase	42	79	—	80

<sup>a</sup> Bond dissociation enthalpies (BDE).

subsequent reduction that gives the amide species. The low driving force for PCET-assisted reduction of nitride **2** can be attributed to an overstabilization that results from strong Re≡N triple bonding.

Besides these thermochemical considerations, an encouraging result is that the amide complex **3** can be readily oxidized even though the first step (formation of **Re=NH**) is uphill. The conversion of **3** to **2** by TEMPO, for instance, occurs within minutes even though the first step is thermodynamically uphill by 3 kcal mol<sup>−1</sup>. The ability of the first H<sup>+</sup> abstraction to proceed indicates that the barriers for the H-atom transfer reactions are low. Therefore, even less stable imide intermediates may be sufficient to allow rapid catalysis in the future.

## Conclusions

Rhenium-amide and -ammine complexes have been isolated, and they are readily oxidized to the corresponding metal-nitride complex. The conversion of NH<sub>3</sub> to a nitride by Re(PNP)Cl<sub>2</sub> (**1**) to form Re(PNP)(N)Cl (**2**) represents the first example of an NH<sub>3</sub>-to-nitride transformation at Re. Since **2** can also be generated *via* electrochemical N<sub>2</sub> cleavage, this system is relevant both to N<sub>2</sub> reduction and ammonia oxidation. Facile, initial deprotonation of NH<sub>3</sub> occurs upon coordination to **1** to form the amide complex Re(PNP)(NH<sub>2</sub>)Cl (**3**). The subsequent conversion to Re≡N can be accomplished with weak hydrogen atom acceptors that provide low driving force for the H<sup>+</sup> transfer, indicating that the reactions are kinetically facile.

Calorimetric measurements of the conversion of **3** to **2** with <sup>t</sup>Bu<sub>3</sub>PhO<sup>+</sup> show that the average BDE<sub>N–H</sub> of **3** in THF is 55.4 ± 1 kcal mol<sup>−1</sup>. This is a rare experimental thermochemical measurement of N–H bond strengths relevant to N<sub>2</sub>/NH<sub>3</sub> interconversions.<sup>76</sup> Computations show that this average is derived from two disparate N–H bond strengths, as the second

N–H BDE in **3** (77 kcal mol<sup>−1</sup>) is much stronger than the N–H BDE in the putative imide intermediate **LRe<sup>IV</sup>=NH** (38 kcal mol<sup>−1</sup>). The ability to form the weak N–H bond in this imide, even transiently, is identified as a crucial bottleneck for N<sub>2</sub> to NH<sub>3</sub> conversion in this system. The combination of bracketing,<sup>46</sup> calorimetry and DFT is a powerful strategy that will continue to elucidate the steps of N<sub>2</sub> reduction at metal complexes.

## Data availability

Crystallographic data have been deposited at the CCDC with deposition numbers 2100974-2100975 and can be obtained from <https://www.ccdc.cam.ac.uk/structures/>. Other data supporting this article have been uploaded as part of the ESI.†

## Author contributions

Conceptualization: G. P. C., J. M. M., P. L. H.; investigation and analysis: G. P. C., D. D., J. E. W., B. Q. M., J. B. C.; writing, interpretation: G. P. C., D. D., J. E. W., S. S., J. M. M., P. L. H.

## Conflicts of interest

There are no conflicts to declare.

## Acknowledgements

We thank the U.S. National Science Foundation (P. L. H. and J. M. M., CHE-1665137, CHE-1954254 and DGE-1752134; J. E. W. and J. B. C., Graduate Research Fellowships) and the Deutsche Forschungsgemeinschaft (S. S., 389479699/RTG2455) for funding.



## Notes and references

† The BDFE of  $t\text{Bu}_3\text{PhO-H}$  in THF has recently been reported as  $74.4 \text{ kcal mol}^{-1}$ ,<sup>69</sup> so the bond dissociation enthalpy (BDE) can be estimated as  $80.7 \text{ kcal mol}^{-1}$ . This takes  $TS^\circ$  for  $\text{H}^\bullet$  in THF to be  $6.3 \pm 0.2 \text{ kcal mol}^{-1}$ , the mean of the  $TS^\circ(\text{H}^\bullet)$  values for moderately polar aprotic solvents.

- 1 V. Smil, *Enriching the Earth: Fritz Haber, Carl Bosch, and the Transformation of World Food Production*, MIT Press, Cambridge, MA, 2004.
- 2 J. W. Erisman, M. A. Sutton, J. Galloway, Z. Klimont and W. Winiwarter, *Nat. Geosci.*, 2008, **1**, 636–639.
- 3 J. N. Renner, L. F. Greenlee, K. E. Ayres and A. M. Herring, *Electrochem. Soc. Interface*, 2015, **24**, 51–57.
- 4 R. F. Service, *Science*, 2018, **361**, 120–123.
- 5 A. J. Martin, T. Shinagawa and J. Perez-Ramirez, *Chem*, 2019, **5**, 263–283.
- 6 N. M. Adli, H. Zhang, S. Mukherjee and G. Wu, *J. Electrochem. Soc.*, 2018, **165**, J3130–J3147.
- 7 O. Elishav, B. Mosevitzky Lis, E. M. Miller, D. J. Arent, A. Valera-Medina, A. Grinberg Dana, G. E. Shter and G. S. Grader, *Chem. Rev.*, 2020, **120**, 5352–5436.
- 8 (a) J. J. Warren, T. A. Tronic and J. M. Mayer, *Chem. Rev.*, 2010, **110**, 6961–7001; (b) R. G. Agarwal, S. C. Coste, B. D. Groff, A. M. Heuer, H. Noh, G. A. Parada, C. F. Wise, E. M. Nichols, J. J. Warren and J. M. Mayer, *Chem. Rev.*, 2022, **122**, 1–49.
- 9 D. R. Weinberg, C. J. Gagliardi, J. F. Hull, C. F. Murphy, C. A. Kent, B. C. Westlake, A. Paul, D. H. Ess, D. G. McCafferty and T. J. Meyer, *Chem. Rev.*, 2012, **112**, 4016–4093.
- 10 G. Hochman, A. S. Goldman, F. A. Felder, J. M. Mayer, A. J. M. Miller, P. L. Holland, L. A. Goldman, P. Manocha, Z. Song and S. Aleti, *ACS Sustainable Chem. Eng.*, 2020, **8**, 8938–8948.
- 11 C. Rebreyend and B. de Bruin, *Angew. Chem., Int. Ed.*, 2015, **54**, 42–44.
- 12 C. J. M. van der Ham, M. T. M. Koper and D. G. H. Hetterscheid, *Chem. Soc. Rev.*, 2014, **43**, 5183–5191.
- 13 V. Rosca, M. Duca, M. T. de Groot and M. T. M. Koper, *Chem. Rev.*, 2009, **109**, 2209–2244.
- 14 V. Kyriakou, I. Garagounis, E. Vasileiou, A. Vourros and M. Stoukides, *Catal. Today*, 2017, **286**, 2–13.
- 15 H. Liu, L. Wei, F. Liu, Z. Pei, J. Shi, Z.-J. Wang, D. He and Y. Chen, *ACS Catal.*, 2019, **9**, 5245–5267.
- 16 Y. Wan, J. Xu and R. Lv, *Mater. Today*, 2019, **27**, 69–90.
- 17 D. V. Yandulov and R. R. Schrock, *Science*, 2003, **301**, 76–78.
- 18 S. Kuriyama, K. Arashiba, K. Nakajima, H. Tanaka, N. Kamaru, K. Yoshizawa and Y. Nishibayashi, *J. Am. Chem. Soc.*, 2014, **136**, 9719–9731.
- 19 K. Arashiba, E. Kinoshita, S. Kuriyama, A. Eizawa, K. Nakajima, H. Tanaka, K. Yoshizawa and Y. Nishibayashi, *J. Am. Chem. Soc.*, 2015, **137**, 5666–5669.
- 20 K. Arashiba, A. Eizawa, H. Tanaka, K. Nakajima, K. Yoshizawa and Y. Nishibayashi, *Bull. Chem. Soc. Jpn.*, 2017, **90**, 1111–1118.
- 21 Y. Ashida, K. Arashiba, K. Nakajima and Y. Nishibayashi, *Nature*, 2019, **568**, 536–540.
- 22 K. Arashiba, Y. Miyake and Y. Nishibayashi, *Nat. Chem.*, 2011, **3**, 120–125.
- 23 L. A. Wickramasinghe, T. Ogawa, R. R. Schrock and P. Muller, *J. Am. Chem. Soc.*, 2017, **139**, 9132–9135.
- 24 T. Itabashi, I. Mori, K. Arashiba, A. Eizawa, K. Nakajima and Y. Nishibayashi, *Dalton Trans.*, 2019, **48**, 3182–3186.
- 25 A. Eizawa, K. Arashiba, A. Egi, H. Tanaka, K. Nakajima, K. Yoshizawa and Y. Nishibayashi, *Chem.-Asian J.*, 2019, **14**, 2091–2096.
- 26 J. S. Anderson, J. Rittle and J. C. Peters, *Nature*, 2013, **501**, 84–87.
- 27 S. E. Creutz and J. C. Peters, *J. Am. Chem. Soc.*, 2013, **136**, 1105–1115.
- 28 T. J. Del Castillo, N. B. Thompson and J. C. Peters, *J. Am. Chem. Soc.*, 2016, **138**, 5341–5350.
- 29 M. J. Chalkley, T. J. Del Castillo, B. D. Matson, J. P. Roddy and J. C. Peters, *ACS Cent. Sci.*, 2017, **3**, 217–223.
- 30 M. J. Chalkley, T. J. Del Castillo, B. D. Matson and J. C. Peters, *J. Am. Chem. Soc.*, 2018, **140**, 6122–6129.
- 31 M. J. Chalkley, M. W. Drover and J. C. Peters, *Chem. Rev.*, 2020, **120**, 5582–5636.
- 32 P. L. Dunn, B. J. Cook, S. I. Johnson, A. M. Appel and R. M. Bullock, *J. Am. Chem. Soc.*, 2020, **142**, 17845–17858.
- 33 K. Dehnicke and J. Strähle, *Angew. Chem., Int. Ed. Engl.*, 1992, **31**, 955–978.
- 34 J. Du Bois, J. Hong, E. M. Carreira and M. W. Day, *J. Am. Chem. Soc.*, 1996, **118**, 915–916.
- 35 R. M. Clarke and T. Storr, *J. Am. Chem. Soc.*, 2016, **138**, 15299–15302.
- 36 M. Keener, M. Peterson, R. Hernandez Sanchez, V. F. Oswald, G. Wu and G. Menard, *Chem. –Eur. J.*, 2017, **23**, 11479–11484.
- 37 B. J. Cook, S. I. Johnson, G. M. Chambers, W. Kaminsky and R. M. Bullock, *Chem. Commun.*, 2019, **55**, 14058–14061.
- 38 P. Bhattacharya, Z. M. Heiden, E. S. Wiedner, S. Rauegi, N. A. Piro, W. S. Kassel, R. M. Bullock and M. T. Mock, *J. Am. Chem. Soc.*, 2017, **139**, 2916–2919.
- 39 G. W. Margulieux, M. J. Bezdek, Z. R. Turner and P. J. Chirik, *J. Am. Chem. Soc.*, 2017, **139**, 6110–6113.
- 40 S. I. Johnson, S. P. Heins, C. M. Klug, E. S. Wiedner, R. M. Bullock and S. Rauegi, *Chem. Commun.*, 2019, **55**, 5083–5086.
- 41 D. W. Pipes, M. Bakir, S. E. Vitols, D. J. Hodgson and T. J. Meyer, *J. Am. Chem. Soc.*, 1990, **112**, 5507–5514.
- 42 G. M. Coia, K. D. Demadis and T. J. Meyer, *Inorg. Chem.*, 2000, **39**, 2212–2223.
- 43 P. Bhattacharya, Z. M. Heiden, G. M. Chambers, S. I. Johnson, R. M. Bullock and M. T. Mock, *Angew. Chem., Int. Ed.*, 2019, **58**, 11618–11624.
- 44 K. Nakajima, H. Toda, K. Sakata and Y. Nishibayashi, *Nat. Chem.*, 2019, **11**, 702–709.
- 45 P. L. Dunn, S. I. Johnson, W. Kaminsky and R. M. Bullock, *J. Am. Chem. Soc.*, 2020, **142**, 3361–3365.





- 46 M. G. Scheibel, J. Abbenseth, M. Kinauer, F. W. Heinemann, C. Wuertele, B. de Bruin and S. Schneider, *Inorg. Chem.*, 2015, **54**, 9290–9302.
- 47 D. D. Thusius and H. Taube, *J. Phys. Chem.*, 1967, **71**, 3845–3857.
- 48 H. Taube and J. D. White, *J. Phys. Chem.*, 1970, **74**, 4142–4149.
- 49 J. D. Buhr and H. Taube, *Inorg. Chem.*, 1979, **18**, 2208–2212.
- 50 J. P. Collman, J. E. Hutchison, M. S. Ennis, M. A. Lopez and R. Guillard, *J. Am. Chem. Soc.*, 1992, **114**, 8074–8080.
- 51 O. Ishitani, P. S. White and T. J. Meyer, *Inorg. Chem.*, 1996, **35**, 2167–2168.
- 52 O. Ishitani, E. Ando and T. J. Meyer, *Inorg. Chem.*, 2003, **42**, 1707–1710.
- 53 M. D. Zott, P. Garrido-Barros and J. C. Peters, *ACS Catal.*, 2019, **9**, 10101–10108.
- 54 F. Habibzadeh, S. L. Miller, T. W. Hamann and M. R. Smith III, *Proc. Natl. Acad. Sci. U. S. A.*, 2019, **116**, 2849–2853.
- 55 M. D. Zott and J. C. Peters, *J. Am. Chem. Soc.*, 2021, **143**, 7612–7616.
- 56 A. Najafian and T. R. Cundari, *J. Phys. Chem. A*, 2019, **123**, 7973–7982.
- 57 S. J. K. Forrest, B. Schluschaß, E. Y. Yuzik-Klimova and S. Schneider, *Chem. Rev.*, 2021, **121**, 6522–6587.
- 58 Q. J. Bruch, G. P. Connor, C.-H. Chen, P. L. Holland, J. M. Mayer, F. Hasanayn and A. J. M. Miller, *J. Am. Chem. Soc.*, 2019, **141**, 20198–20208.
- 59 I. Klopsch, M. Finger, C. Wuertele, B. Milde, D. B. Werz and S. Schneider, *J. Am. Chem. Soc.*, 2014, **136**, 6881–6883.
- 60 B. M. Lindley, R. S. van Alten, M. Finger, F. Schendzielorz, C. Würtele, A. J. M. Miller, I. Siewert and S. Schneider, *J. Am. Chem. Soc.*, 2018, **140**, 7922–7935.
- 61 R. S. van Alten, F. Wätjen, S. Demeshko, A. J. M. Miller, C. Würtele, I. Siewert and S. Schneider, *Eur. J. Inorg. Chem.*, 2020, **2020**, 1402–1410.
- 62 I. Klopsch, M. Kinauer, M. Finger, C. Würtele and S. Schneider, *Angew. Chem., Int. Ed.*, 2016, **55**, 4786–4789.
- 63 I. Klopsch, F. Schendzielorz, C. Volkmann, C. Würtele and S. Schneider, *Z. Anorg. Allg. Chem.*, 2018, **644**, 916–919.
- 64 A. Earnshaw, B. N. Figgis, J. Lewis and R. D. Peacock, *J. Chem. Soc.*, 1961, 3132–3138, DOI: 10.1039/JR9610003132.
- 65 J. Chatt, G. J. Leigh and D. M. P. Mingos, *J. Chem. Soc. A*, 1969, 1674–1680.
- 66 G. P. Connor, B. Q. Mercado, H. M. C. Lant, J. M. Mayer and P. L. Holland, *Inorg. Chem.*, 2019, **58**, 10791–10801.
- 67 G. L. Hillhouse and J. E. Bercaw, *J. Am. Chem. Soc.*, 1984, **106**, 5472–5478.
- 68 B. M. Lindley, Q. J. Bruch, P. S. White, F. Hasanayn and A. J. M. Miller, *J. Am. Chem. Soc.*, 2017, **139**, 5305–5308.
- 69 C. F. Wise, R. G. Agarwal and J. M. Mayer, *J. Am. Chem. Soc.*, 2020, **142**, 10681–10691.
- 70 S. Tshepelevitsh, A. Kütt, M. Lökov, I. Kaljurand, J. Saame, A. Heering, P. G. Plieger, R. Vianello and I. Leito, *Eur. J. Org. Chem.*, 2019, **2019**, 6735–6748.
- 71 C. R. Waidmann, A. J. M. Miller, C.-W. A. Ng, M. L. Scheuermann, T. R. Porter, T. A. Tronic and J. M. Mayer, *Energy Env. Sci.*, 2012, **5**, 7771–7780.
- 72 D. Delony, M. Kinauer, M. Diefenbach, S. Demeshko, C. Würtele, M. C. Holthausen and S. Schneider, *Angew. Chem., Int. Ed.*, 2019, **58**, 10971–10974.
- 73 J. Abbenseth, D. Delony, M. C. Neben, C. Würtele, B. de Bruin and S. Schneider, *Angew. Chem., Int. Ed.*, 2019, **58**, 6338–6341.
- 74 M. J. Bezdek, S. Guo and P. J. Chirik, *Science*, 2016, **354**, 730–733.
- 75 M. J. Bezdek and P. J. Chirik, *Angew. Chem., Int. Ed.*, 2018, **57**, 2224–2228.
- 76 M. J. Bezdek, I. Pappas and P. J. Chirik, in *Nitrogen Fixation*, ed. Y. Nishibayashi, Springer International Publishing, Cham, 2017, pp. 1–21, DOI: 10.1007/3418\_2016\_8.
- 77 B. D. Matson and J. C. Peters, *ACS Catal.*, 2018, **8**, 1448–1455.
- 78 G. C. Stephan, C. Sivasankar, F. Studt and F. Tuczek, *Chem. –Eur. J.*, 2008, **14**, 644–652.
- 79 D. Wang, F. Loose, P. J. Chirik and R. R. Knowles, *J. Am. Chem. Soc.*, 2019, **141**, 4795–4799.
- 80 I. Pappas and P. J. Chirik, *J. Am. Chem. Soc.*, 2016, **138**, 13379–13389.
- 81 N. M. Adli, H. Zhang, S. Mukherjee and G. Wu, *J. Electrochem. Soc.*, 2018, **165**, J3130–J3147.
- 82 M. Keener, M. Peterson, R. Hernandez Sanchez, V. F. Oswald, G. Wu and G. Menard, *Chem. –Eur. J.*, 2017, **23**, 11479–11484.
- 83 W.-L. Man, T.-M. Tang, T.-W. Wong, T.-C. Lau, S.-M. Peng and W.-T. Wong, *J. Am. Chem. Soc.*, 2004, **126**, 478–479.
- 84 M. G. Scheibel, Y. Wu, A. C. Stückl, L. Krause, E. Carl, D. Stalke, B. de Bruin and S. Schneider, *J. Am. Chem. Soc.*, 2013, **135**, 17719–17722.
- 85 J. Abbenseth, M. Finger, C. Wuertele, M. Kasanmascheff and S. Schneider, *Inorg. Chem. Front.*, 2016, **3**, 469–477.
- 86 M. G. Scheibel, B. Askevold, F. W. Heinemann, E. J. Reijerse, B. de Bruin and S. Schneider, *Nature Chem.*, 2012, **4**, 552–558.
- 87 M. J. Chalkley, P. H. Ojala and J. C. Peters, *J. Am. Chem. Soc.*, 2019, **141**, 4721–4729.

